Flow and Topographic Changes in Compound Meandering Rivers

Shoji Fukuoka[1]

Abstract

Flood flow in compound meandering channels exhibits flow storage and attenuation of peak discharge. A sufficient understanding of these characteristics is essential for river design projects that include assessment of dam reservoir and capacity flood relief schemes. Laboratory experiments in a compound meandering channel were performed and flood data from Ota River were analyzed. Results of comparison of the experimental and Ota River data indicated similar characteristics of flood flow storage. Assessing both channel storage capacity and peak discharge attenuation mechanism, a new concept of flood control plans is presented.

Additionally, for the evaluation of the structure of flows and river bed topography in a compound meandering channel, a three dimensional numerical model was developed. The numerical model can evaluate and reproduce accurately the features of the flow field and bed topography observed in compound meandering channels. It was considered that the use of a non-hydrostatic pressure model is necessary for evaluating the deformation in a compound meandering channel with high relative depth values. The numerical analysis has shown the importance of secondary flow structures in the formation of the bed features.

Keywords: floodflow, compound meandering channel, channel storage, 3-D numerical model, bed topography

1 Introduction

Depending on a channel's planform and cross-sectional shape, it is known that a flood flow whose discharge changes temporally is stored as it proceeds downstream, resulting in transformation of discharge and water level hydrograph such as in the peak discharge attenuation (Chow, 1956; Fukuoka, 1999; Fukuoka, et al. 2000). In a channel with a uniform cross-section, the shape of flood wave is

1 Professor, Department of Civil and Environmental Engineering, Hiroshima University, Higashi Hiroshima, 739-8527, Japan

transformed into a mild one in the process of the downstream propagation because of the time change in hydraulic quantities. On the other hand, in a flood flow the peak discharge attenuation is caused by the channel storage function inherent in an unsteady non-uniform flow. Because little is known about the relationship of flood flow characteristics and channel storage characteristics, however, the natural flood flow storage capacity of rivers has yet to be reflected in flood control plans. Large rivers with broad floodplain and complex planforms are assumed to have considerable storage capacity. Furthermore, although vegetation that grows in channels is often cleared for the reason that, during flooding, such vegetation raises water levels and lowers a channel's discharge capacity. Large rivers with sufficient embankment height are amenable to measures that conserve channel vegetation not just because of its environmental functions, but also to increase flood flow storage in the channel. Fukuoka et al. (2000) studied by experiment the effects on the hydraulic properties of food flows on planform, transverse shape, and unsteadiness in the compound meandering rivers commonly seen in Japan, thus gaining a basic understanding of these effects.

Flow in a compound meandering channel were found to differ greatly from those of bankful flow when the water depth over the floodplain is large, by Ashida et al. (1989, 1990), Kinoshita (1988), Mori et al. (1989), Willet et al. (1993) and Sellin et al. (1993). Among these differences, the maximum velocity filament in the main channel runs near the inner banks; regarding the secondary flows, the rotation is reversed from that observed in bankful flows (Fukuoka et al., 1996; Muto et al., 1997). These changes in the flow fields are accompanied by the cessation of scouring at outer bank bed and by the scouring near the inner bank bed (Fukuoka et al. 1997a). It is generally believed that these flow characteristics are depending on the sinuosity and the phase difference between the main channel alignment and the levee alignment, the relative depth, the ratio of roughness and width between flood channel and main channel, and so on. The effects of relative depth and sinuosity were shown by means of the large-scale hydraulic experiments performed by Fukuoka et al. (1997a, 1997b) and the flow velocity distributions calculated from actual aerial survey photographs (Fukuoka et al., 1997c).

The geometrical and hydraulic conditions affect dramatically the features of the flow structure in a compound meandering channel, therefore numerical analysis should be used to compute flow and bed evolution. Efforts were made to develop three-dimensional numerical models of compound meandering flows. The authors developed a numerical model that used the spectral method to express three dimensional flows in compound meandering channels with fixed bed (Fukuoka et al., 1998; Watanabe et al., 1999.) and it is able to express the changes in the structure of flow due to the changes in the relative depth.

In this paper, the author has taken a further step on the research of Fukuoka et al. (1999), performing systematic experiment on flood flows in a compound meandering channel and analyzing flood observation data for the Ota River with the objective of estimating a channel's storage capacity of a flood. Assessing both channel storage capacity and peak discharge attenuation mechanism, a new approach to flood control plans is presented.

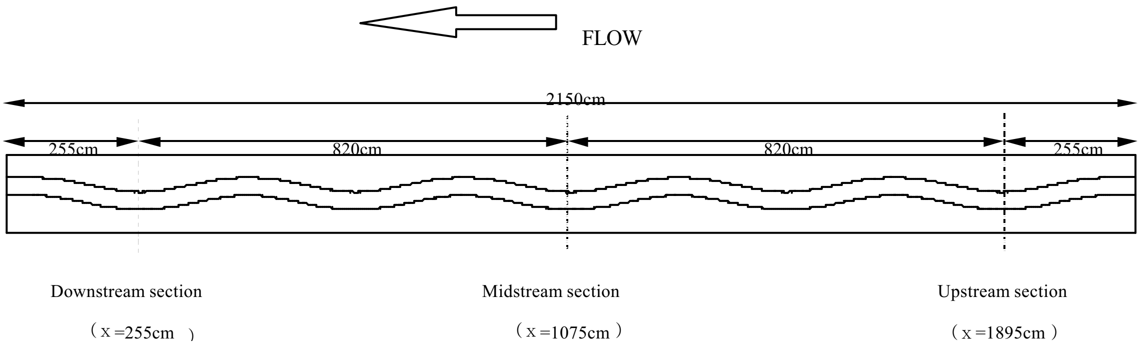

Fig. 1. Plan view of experimental channel used

Table 1. Specifications of experimental channel

Channel length	Total channel width	Main channel width	Channel bed slope	Sinuosity	Meander wavelength	Flood channel height
2150 (cm)	220 (cm)	50 (cm)	1/1000	1.02	410 (cm)	4.5 (cm)

Table 2. Hydrograph properties

Case	Peak discharge	Maximum relative depth	Duration of flood channel inundation	Duration of rising water period	River equivalent of peak discharge	River equivalent of duration of flood channel inundation
Case1 , 3 (Hydro A)	17 (l/sec)	0.4	1200 (sec)	600 (sec)	9,622 (m^3/sec)	4.7 (hr)
Case2 (Hydro B)	18 (l/sec)	0.41	3500 (sec)	1000 (sec)	10,188 (m^3/sec)	13.6 (hr)
1983 flood in Tone River (Kurihashi)	8,100 (m^3/sec)	0.56	64 (hr)	—	—	—

This paper also describes the numerical analysis model incorporating bed variations into a 3-D flow model (Fukuoka et al., 1998; Watanabe et al., 1999) and discusses its suitability for flow and bed variation against the change in the relative depth. A flow model of non-hydrostatic pressure mode is used to examine the significance of change in pressure intensity.

2 Flood Flow Storage and Peak Flow Attenuation in Channels

2.1 Method of experiment

A large open channel having a compound meandering shape (Fig. 1) was used in experiment to assess the mechanism of flood wave propagation, storage capacity, and peak discharge attenuation. Table 1 shows the specifications of the experimental channel used. The floods flow having the hydrographs (Hydro A and Hydro B) indicated in Fig. 5 by solid lines were released from the upstream end of the channel. Table 2 shows the characteristics of each hydrograph and those of a 1983 flood in the Tone

River. Assuming the channel to be a 1/200-scale model, the experimental hydrograph generally satisfies Froude similarity law of flood flows in actual rivers (Fukuoka, 2000). The downstream discharge (Q_{out}) hydrograph was calculated from the temporal change in storage capacity (dS/dt), which was calculated from the temporal change in the longitudinal water level simultaneously measured between the upstream and downstream sections, and from the inflow discharge (Qin) hydrograph for each corresponding time.
Water level was measured with a servo-type wave gage meter; velocity, with a type I electromagnetic velocimeter. The longitudinal distribution of water level was measured between the aforesaid upstream and downstream cross-sections, whereas the transverse distribution of velocity was measured at the midstream cross-section (x = 1,075 cm) (Fig. 2).

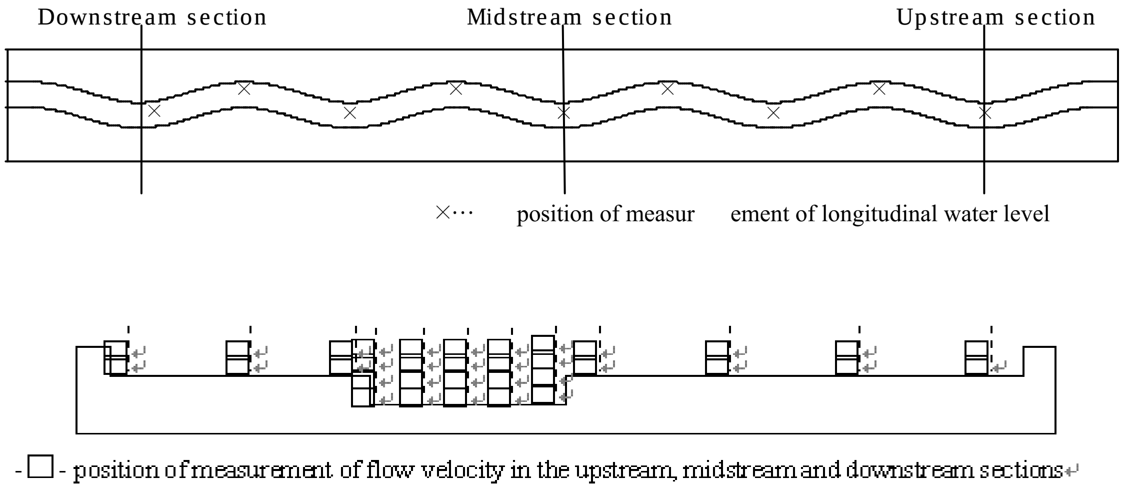

Fig. 2. Points of measurement of water level and flow velocity

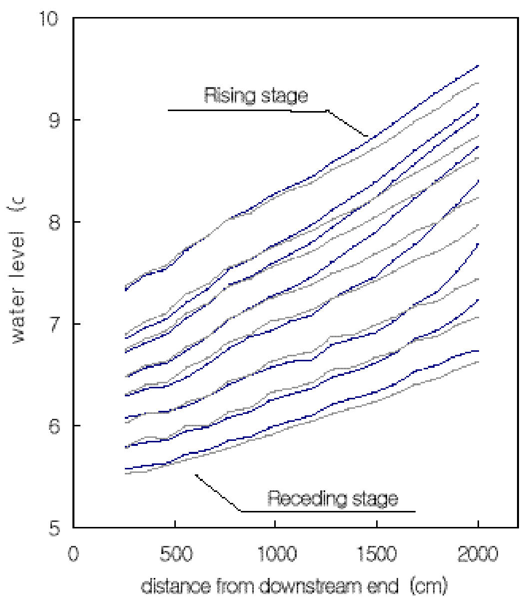

Fig. 3. Longitudinal water level distribution for Case 1

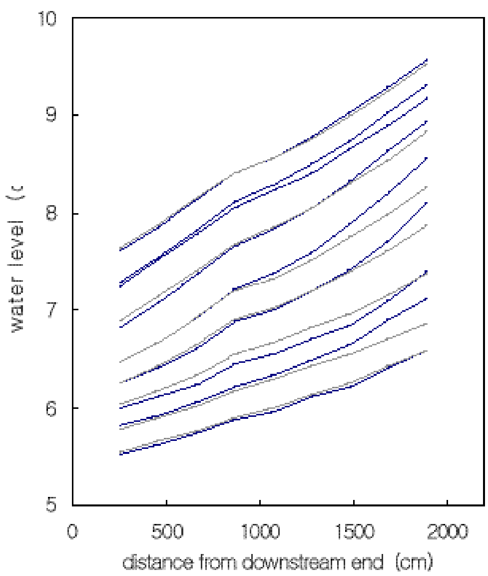

Fig. 4. Longitudinal water level distribution for Case2

2.2 Conditions of experiment

The author performed the experiment under three different sets of conditions. Case 1 employed an isosceles triangular hydrograph (Hydro A), and Case 2 a hydrograph (Hydro B) with relatively less unsteadiness than in Case 1. In Case 3, the same hydrograph (Hydro A) as that in Case 1 was used, and vegetation was placed in the flood channel of a compound meandering channel to investigate the effects of riparian vegetation on storage volume.

At the downstream end of the channel, a porous plastic body (porosity = 91%) was installed to create sufficient resistance so that depth near the downstream end in each time would approach nearly uniform flow depth.

2.3 Results and considerations

(1) Effect of unsteadiness

Figs. 3 and 4 show the temporal change in the longitudinal water level in Case 1 (Hydro A) and Case 2 (Hydro B). This is shown for the times, during the rising water period (solid line) and receding water period (broken line), at which the downstream end water level was the same. These graphs demonstrate that water surface slope is steep during the rising water period but gentle during the receding water period; the mechanism of flood wave propagation is also evident in channel experiment, and that high unsteadiness (i.e., Hydro A) results in marked changes in water surface slope.

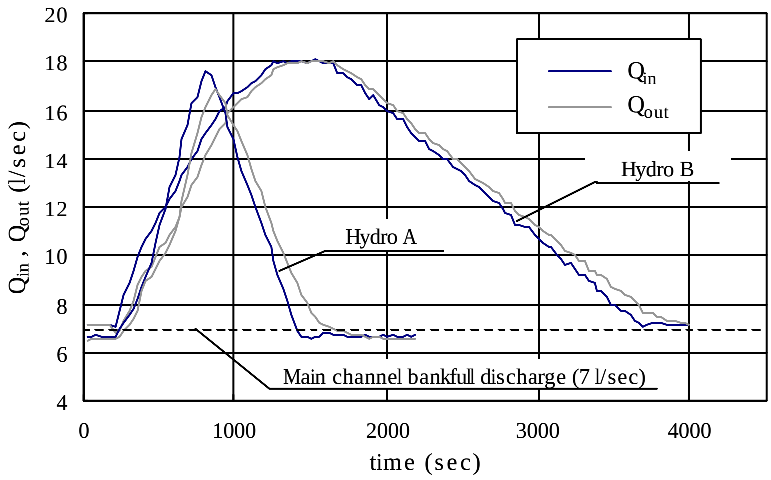

Fig. 5. Comparison of upstream and downstream discharges

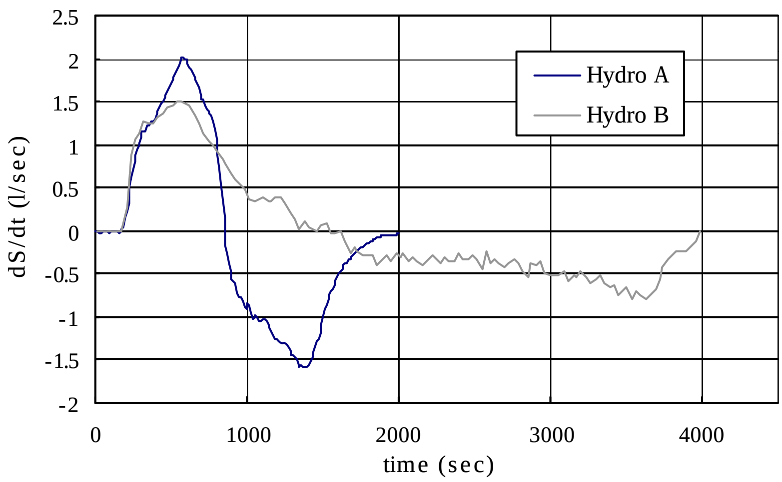

Fig. 6. Changes in the ratio of dS/dt to inflow discharge

Fig. 5 shows the discharge hydrographs for the upstream section (where x = 1,895 cm) and the downstream section (where x = 255 cm). These discharge hydrographs suggest that as the flow moves downstream, it is subjected to the effects of flood channel roughness, main channel alignment, and mixing of the main channel and flood channel flows, the result being that the downstream section indicates transformation in the flood hydrograph, i.e., attenuation of the peak discharge, delaying of the occurrence of peak discharge, and prolonging of the flood duration. Such hydrograph changes are prominent in high-unsteadiness Hydro A. Temporal delaying of the discharge hydrograph and the attenuation of maximum discharge occur primarily because of storage of the flood flow. Storage capacity per unit time (dS/dt) is obtained by subtracting discharge Q_{out}, from discharge Q_{in}. Fig. 6 gives the ratio of temporal change in storage to inflow discharge Q_{in}. On the positive side of the graph, the value of Q_{out} is less than that of Q_{in}, and so the flood flow is stored within the channel. Subsequently, on the negative side, Q_{in} falls below Q_{out}, and so the discharge that had been stored within the channel now flows out. In Hydro A, dS/dt at the time of peak discharge inflow is 5% of Q_{in}, whereas maximum dS/dt is 15% of Q_{in}.

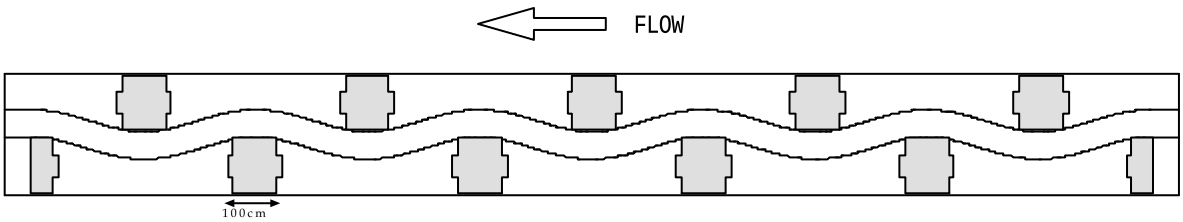

Fig. 7. Vegetation placed on the inner bank of the meander channel

(2) Effect of riparian vegetation

To investigate the storage effect of vegetation, the author, as Fig. 7 shows, installed a continuous cover of vegetation on the inner bank of the meander, in the broad portion of the flood channel, where storage effect was assumed to be greatest. This configuration of vegetation, by decreasing the cross-sectional area of the flood channel, created resistance to the flow and so raised water levels.

Figs. 8 shows the longitudinal water level distribution for Case 3, in which vegetation was placed. Fig. 9, which is temporal change in the water surface slope in the channel 's central section (i.e., the section 1,485 to 665 cm from the downstream end), shows a marked increase in water surface slope in Case 3, relative to Case 1 of Fig.3, in which no vegetation was placed. In Case 1, peak surface slope occurred at the time of large mixing between the flow in the flood channel and the flow in the main channel which characterizes a compound meandering channel flow. In contrast, peak surface slope occurs in Case 3, decrease of the peak water depth, where the effect of the vegetation is greatest. Figs. 10 and 11 are the depth/discharge curve and depth/main channel average velocity curve for central cross-section of the channel. In Case 3, the depth/discharge curve describes a much larger loop than in Case 1 because of a surface slope that is

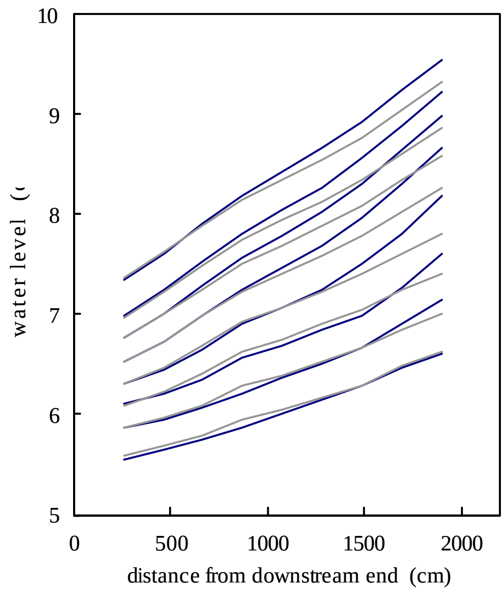

Fig. 8. Longitudinal water level distribution for Case 3

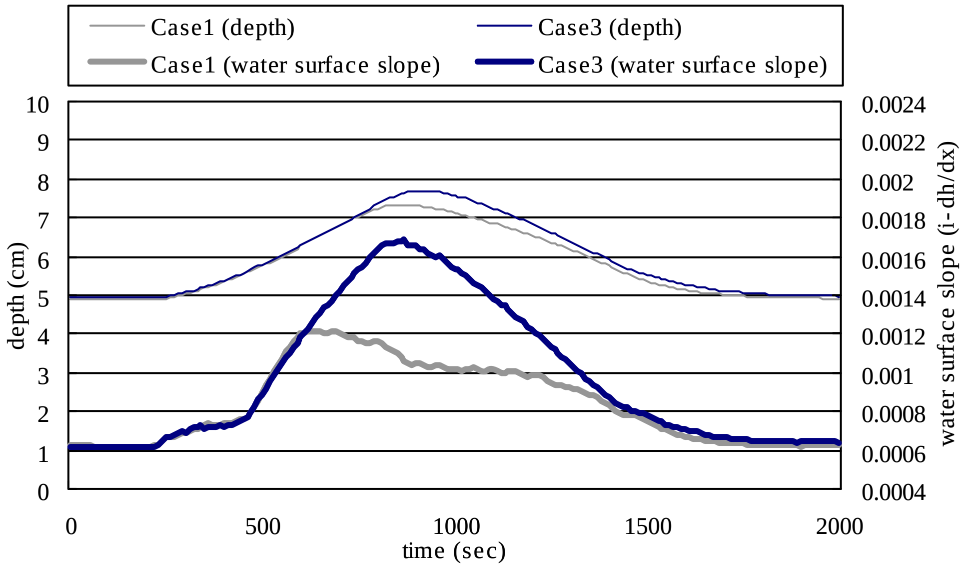

Fig. 9. Water depth and water surface slope hydrographs

larger due to the effects of the vegetation. This demonstrates that, even under identical unsteady input conditions, factors that make a channel's surface slope change will result in a larger loop for the depth/discharge curve. The depth/main channel average velocity curve also shows that in Case 1, surface slope peaks at a depth of 5.5 to 6.0 cm, where the mixing effects of the compound meandering flow are great, and that main channel average velocity also peaks at the same time. In Case 3, in contrast, because the effects of vegetation increase along as flood channel depth increases, velocity peaks near maximum surface slope and maximum depth.

Fig. 12, which is a hydrograph of inflow and outflow in Cases 1 and 3, shows that the attenuation of peak discharge at the downstream section is approximately twice as high in Case 3 than in Case 1.

Fig. 13 gives the temporal change in storage (dS/dt) in relation to Q_{in}, and shows that in Case 3, the ratio is higher than in Case 1, as much as 12% to 13% of the flood flow is stored during the rising water period. This diagram also indicates that when peak discharge occurs

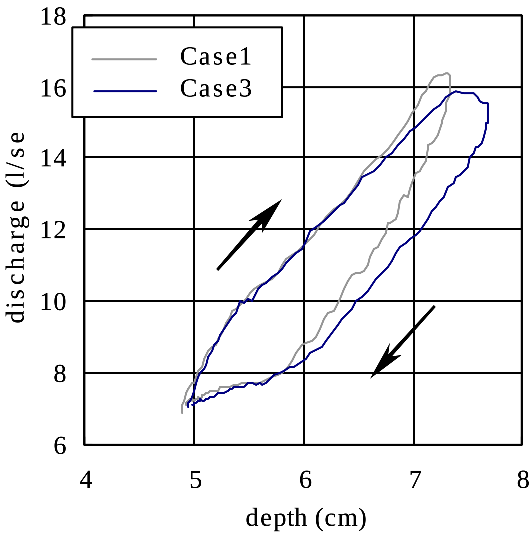

Fig. 10. Depth-discharge curve

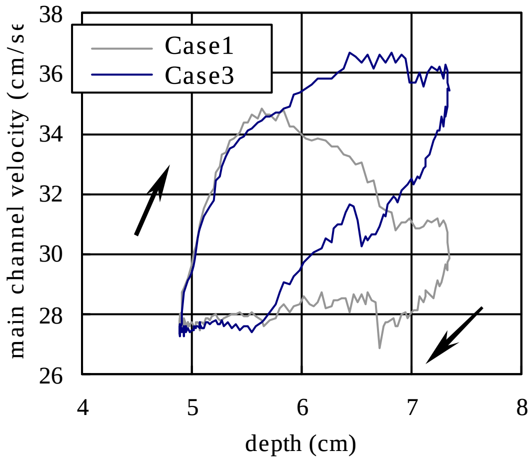

Fig. 11. Depth-main channel velocity curve

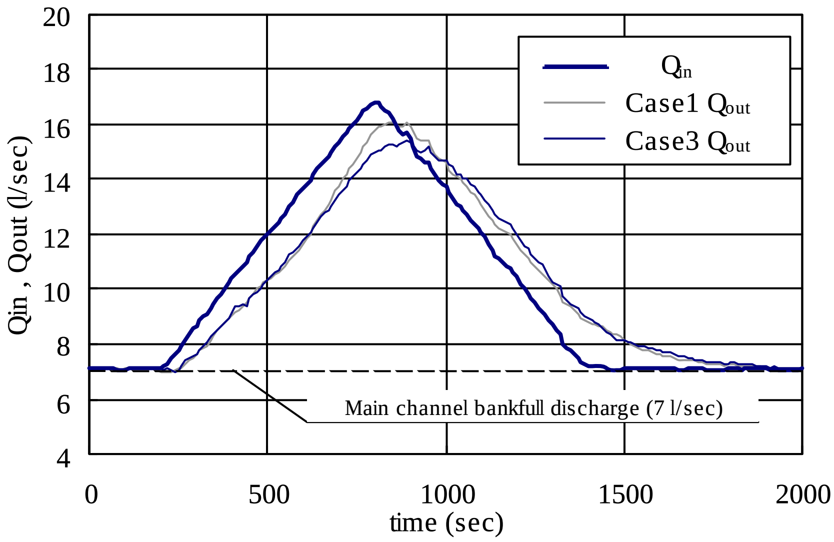

Fig. 12. Comparison of inflow discharge and outflow discharge for Cases 1 and 3

at the upstream section, dS/dt was 6.2% relative to Q_{in} in Case 1, but was 10.7% in Case 3. This clearly shows that riparian vegetation increases both flood flow storage and attenuation of peak disctharge.

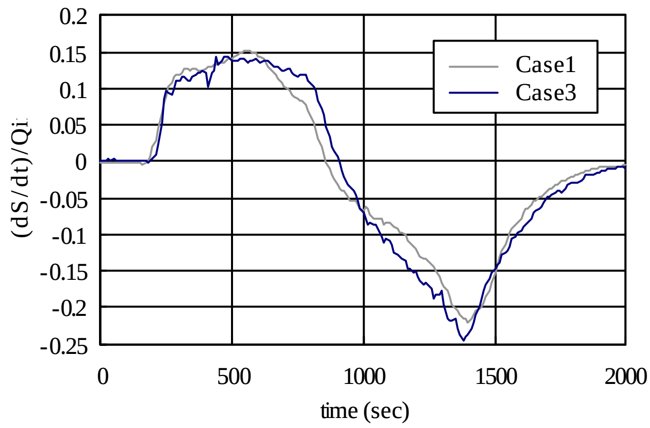

Fig. 13. Temporal change in the ratio dS/dt to inflow discharge

(3) Comparison of the results of flood flow experiment and the observation results of ota river flood

Figs. 14 and 15 show, with broken lines, the results of analysis of flood observation data obtained at the Yaguchi Observation Post No. 1 (located 11.6 km upstream from the river's mouth) during July 1983 flooding. In these graphs, the results from the main channel Case 1 are indicated with a solid line. With regards to the relationship of water level to average velocity and discharge, water level is nondimensionalized with peak water level h_{max}, assuming a water level of zero to be the height of the flood channel h_f; velocity and discharge are nondimensionalized with their respective peak values. The arrows in

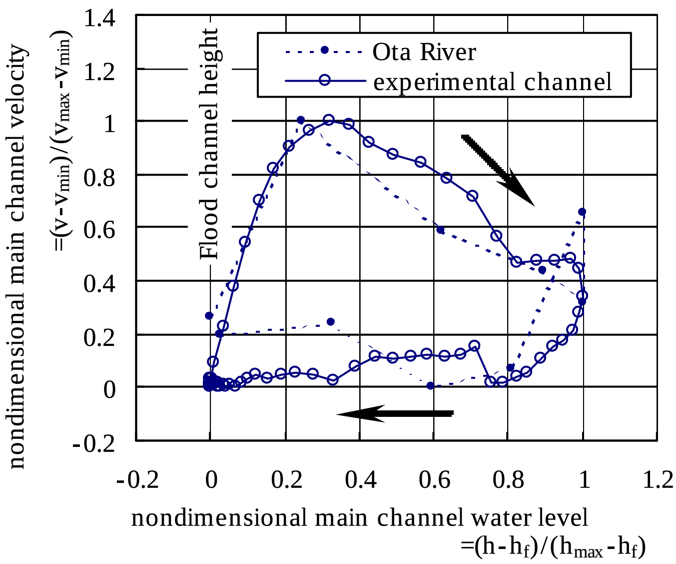

Fig. 14. Nondimensional depth-velocity curve for Ota River and experimental channel

the graphs indicate the passage of time.

Figs. 16 and 17 give plan and cross-sectional views and flood hydrograph of the Ota River observation station; Table 3, the characteristics of the flood hydrograph. At the observation station, located in a compound, gently meandering reach of the river, a water level-main channel velocity and water level-discharge relationship indicate roughly the same characteristics as those of the experiments. This suggests that channel storage occurred during flooding in the Ota River. In order to assess the channel storage capacity of the Ota River, it is, however, necessary to measure the discharge at either upstream or downstream within the reach in question and the temporal change in the longitudinal water level during a flood as shown in Figs.3.4 and 8.

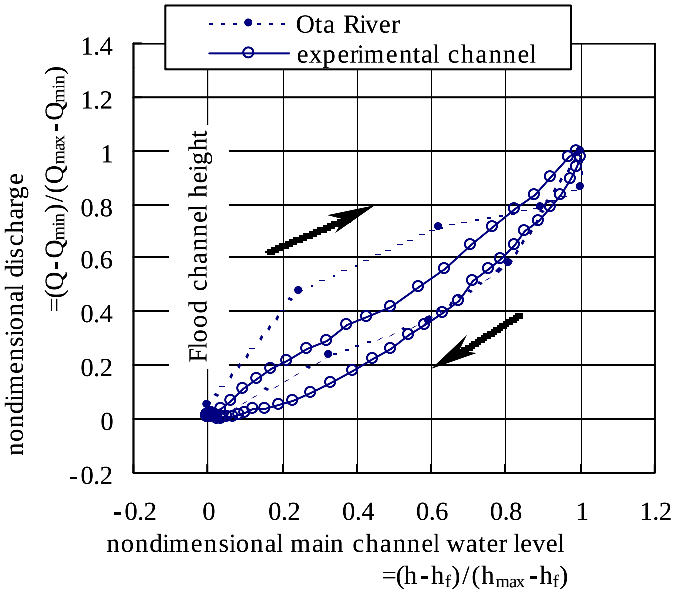

Fig. 15. Nondimensional depth-main channel velocity curve for Ota River and experimental channel

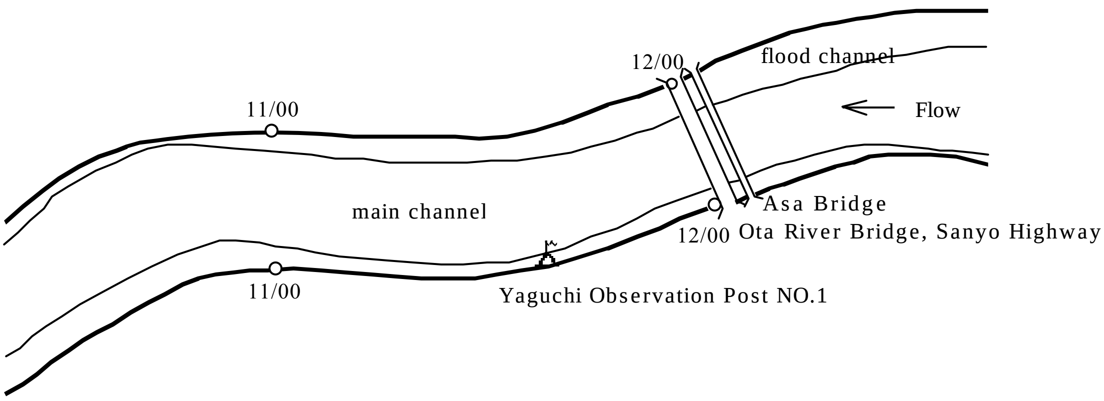

Fig. 16. Plan view of the Yaguchi Observation Post NO.1

Table 3. Characteristics of the 1983 Ota River flood

Flood case	Maximum relative depth	Real river equivalent peak discharge	Real river equivalent flood channel inundation time
Case1 (Hydro A)	0.4	9,622 (m^3/sec)	4.7 (hr)
1983 Ota River flood (Yaguchi Observation Post No. 1)	0.34	3,500 (m^3/sec)	6 (hr)

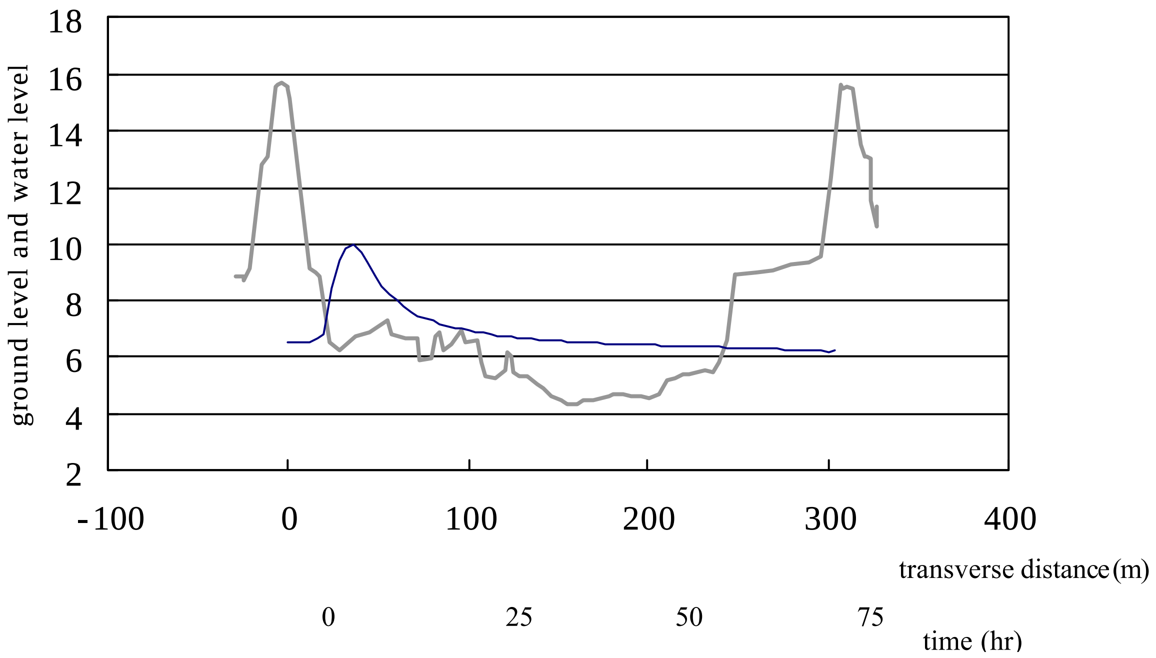

Fig. 17. Cross-section at the Yaguchi Observation Post No.1 and water level hydrograph

3 Numerical Analysis on Three Dimensimal Flow and Bed Topography

3.1 Method of analysis

(1) Introduction of the plane curvilinear coordinate system and σ coordinate system

Coordinate transformation is used as a simple way to incorporate the effects of the complex boundary profile into the numerical analysis. Fig. 18 shows the computation domain of the compound meandering channel to be analyzed, together with the coordinate system. The plane coordinate systems are transformed from rectangular ones (x, y) to curvilinear ones (ξ, η). As shown in Fig.19, the vertical coordinate system z is transformed into σ coordinate system, which is defined as

$$\begin{cases} z = z_o + (z_o - z_p)\sigma, & (\sigma \geq 0) \\ z = z_p + (z_p - z_b)\sigma, & (\sigma < 0) \end{cases} \tag{1}$$

where z_o, z_p and z_b represent the reference plane near the water surface, flood channel and bed heights respectively. The values σ= 1, 0, -1 represent the reference plane for water surface, flood channel and bed heights, respectively. At this time, the scale parameters relating to the vertical axis are respectively represented by using depths above and below a flood channel. If z_o and z_p are constant, the metric tensors can be evaluated from changes in the bed surface or the depth below the flood channel alone, without having to incorporate mesh movement. Thus, a coordinate system results in the following metric tensor matrix.

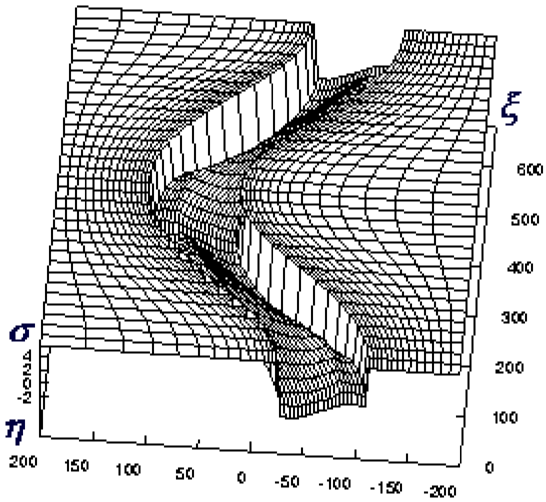

Fig. 18. Coordinate system and computational domain
for compound meandering channel with movable bed. (Length unit: cm)

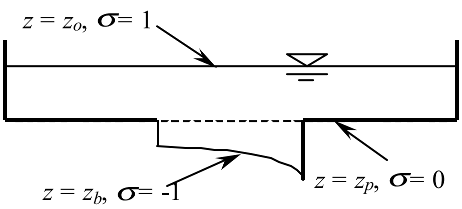

Fig. 19. Definition of σ coordinate system.

$$\begin{bmatrix} \xi_x & \eta_x & \sigma_x \\ \xi_y & \eta_y & \sigma_y \\ \xi_z & \eta_z & \sigma_z \end{bmatrix} =$$

$$\begin{bmatrix} y_\eta / J' & -y_\xi / J' & -(z_\xi \xi_x + z_\eta \eta_x)/z_\sigma \\ -x_\eta / J' & x_\xi / J' & -(z_\xi \xi_y + z_\eta \eta_y)/z_\sigma \\ 0 & 0 & 1/z_\sigma \end{bmatrix} \tag{2}$$

$$J = J' z_\sigma, \quad J' = x_\xi y_\eta - x_\eta y_\xi \tag{3}$$

Where subscripts in the coordinate system indicate the partial differentiation of that coordinate, t represents time, and J the Jacobian. Contravariant flow velocity is represented in the curvilinear coordinate system as follows:

$$\begin{cases} U = \xi_x u + \xi_y v \\ V = \eta_x u + \eta_y v \\ W = \sigma_z W' = \sigma_z (\sigma_x ' u + \sigma_y ' v + w) \end{cases} \tag{4}$$

Where u = x-direction flow velocity; v = y-direction flow velocity; w = z-direction flow velocity; U = ξ-direction contra-variant flow velocity; V = η-direction contra-variant flow velocity and W = σ-direction contra-variant flow velocity. In Equation 4, σ_x' and σ_y' represent the quantities defined by $\sigma_x = \sigma_x' \sigma_z$ and $\sigma_y = \sigma_y' \sigma_z$.

(2) Basic equations of the flow

When the coordinate system is introduced as described above, the equation of motion that expresses the non-hydrostatic pressure is as follows:

$$\frac{\partial u}{\partial t} + U_j \frac{\partial u}{\partial \xi_j} = g_x - g\xi_{j,x} \frac{\partial \zeta}{\partial \xi_j} + \upsilon_T \Delta u - \frac{1}{\rho} \xi_{j,x} \frac{\partial p}{\partial \xi_j} \tag{5a}$$

$$\frac{\partial v}{\partial t} + U_j \frac{\partial v}{\partial \xi_j} = g_y - g\xi_{j,y} \frac{\partial \zeta}{\partial \xi_j} + \upsilon_T \Delta v - \frac{1}{\rho} \xi_{j,y} \frac{\partial p}{\partial \xi_j} \tag{5b}$$

$$\frac{\partial w}{\partial t} + U_j \frac{\partial w}{\partial \xi_j} = g_z - \frac{1}{\rho} \sigma_z \frac{\partial p}{\partial \sigma} + \upsilon_T \Delta v$$

(5c)

$$\Delta = \frac{\partial^2}{\partial x_j^2} \qquad (j = 1,2,3)$$

Where g_x, g_y, g_z = gravitational acceleration in the respective directions, ζ = water level fluctuation relative to the reference surface, p = deviation pressure from the hydrostatic pressure. The eddy viscosity ν_T is expressed in the following equation using h = depth from the reference surface, z_d = height from the bottom, and u_* = bottom friction velocity.

$$\nu_T = \kappa u_* z_d (1 - z_d / h) \tag{6}$$

The continuity equation is expressed as

$$\frac{\partial J U_j}{\partial \xi_j} = 0 \tag{7}$$

Integration of Equation 7 from the bed level (σ =-1) to the water surface ($z = z_o + \zeta$) yields:

$$J'\frac{\partial \zeta}{\partial t} + \frac{\partial}{\partial \xi_k} \int_{-1}^{\sigma(z_o+\zeta)} J' z_\sigma U_k d\sigma = 0 \quad (k = 1,2) \tag{8}$$

The kinematics boundary conditions at the water surface is are given by using the contra-variant flow velocity W' in the σ -direction by Equation 9:

$$\frac{\partial \zeta}{\partial t} + U_k \frac{\partial \zeta}{\partial \xi_k} = W', \quad (z = z_o + \zeta) \tag{9}$$

In the analysis without the assumption of hydrostatic pressure, the deviation pressure p is solved quickly in the spectral space by using SMAC method for Equation 5 and 7 (Fukuoka et al., 1998). The distribution of vertical velocity w is given by the integral of Equation 7 from the bottom.

(3) Basic equations of the bed deformation

The bed variation is expressed by using the sediment continuity equation as follows:

$$J'\frac{\partial z_b}{\partial t} + \frac{1}{1-\lambda}\left(\frac{\partial J' q_{B\xi}}{\partial \xi} + \frac{\partial J' q_{B\eta}}{\partial \eta}\right) = 0 \tag{10}$$

Where ($q_{B\xi}$, $q_{B\eta}$) is the contra-variant sediment discharge vector as given by

$$\begin{cases} q_{B\xi} = q_B\left\{\dfrac{U_b}{\sqrt{u_{kb}^2}} - \dfrac{1}{\sqrt{\mu_s \mu_k}} \dfrac{u_{*c}}{u_*}\left(\xi_{1,i}\xi_{k,i}\dfrac{\partial z_b}{\partial \xi_k}\right)\right\} \\ q_{B\eta} = q_B\left\{\dfrac{V_b}{\sqrt{u_{kb}^2}} - \dfrac{1}{\sqrt{\mu_s \mu_k}} \dfrac{u_{*c}}{u_*}\left(\xi_{2,i}\xi_{k,i}\dfrac{\partial z_b}{\partial \xi_k}\right)\right\} \end{cases} \quad (i,k = 1,2) \tag{11}$$

Equation 11 is obtained through the coordinate transformation of the longitudinal and transverse sediment discharge vector (Fukuoka et al., 1993). The effects of the bed gradient are incorporated in Equation 11. Here, q_B = bed load, μ_s = static friction factor, μ_k = dynamic friction factor, u_{*c} = critical friction velocity, and the subscript b indicates the value at the bed. This analysis takes account of additional tractive force and changes in critical tractive force (Fukuoka et al., 1983) due to the longitudinal and lateral bed slope change for sediment discharge calculation.

(4) Introduction of spectral method and method of calculation

Because the profile of the boundary in a compound meandering channel is changed periodically in the longitudinal direction, Fourier series expanded from the 0th mode to the 7th mode are applied for the plane boundary profile, the flow field and the bed profile in this direction. The spectral collocation method is employed to solve the differential equation in the longitudinal direction. As shown in Fig 18, 32 spectral collocation points were selected.

For the flow field analysis, a longitudinal differentiation was calculated by differentiating in the spectral space and then the value was inverting to the spectral collocation point through inverse Fourier transformation. The convective terms in (η, σ) plane were differentiated using an upwind difference of 1st and 3rd order in the vertical and transverse direction, respectively.

Using the procedure outlined above, velocities u, v, w, pressure p and water level ζ are calculated on the spectral points and then time-integrated in spectral space. The time integrals of velocity and water level are explicitly calculated with the Huen method having 2nd order accuracy in time. The bed deformation is very slow in comparison with the velocity change, therefore, the time variations of bed and velocity are repeatedly calculated at separate time scales in this analysis.

The resistance at the walls is taken proportional to the square of the velocity near the wall, being assigned as a boundary condition for velocity. Impermeable slip-conditions are also applied at the walls. Friction velocities on the walls and the bottom are determined by dividing velocities near the walls and the bed by the resistance coefficient, respectively.

3 .2 Flow and bed deformation analysis

(1) Conditions for experiment and calculation

The plane profile of the compound channel is shown in Figure 18, where the total width = 4.0 m; main channel width = 0.8 m; mean main channel bank height = 0.055 m; meander length = 6.8 m; and sinuosity = 1.1. There are five and two vertical calculation points below and above the flood channel height, respectively.

The author analyzed Cases 4 and 5 in the large-scale laboratory experiments by Fukuoka et al. (1997b). The experimental channel was 15 m long. The flood channel was covered with artificial turf to create the appropriate roughness and the main channel was filled with sand 0.8 mm in diameter. The slope of the channel bed was 1/600. The resistance coefficient at the bottom was calculated by using the equivalent roughness k_s and $z_{1/2}$ using Equation 12.

$$\varphi_b = 5.75\log(z_{1/2}/k_s)+8.5 \tag{12}$$

Where, $z_{1/2}$ is the height in the center, the calculation point for flow velocity, of the 1st bottom mesh. It was assumed that k_s= 2.8 cm in the flood channel. The value of the sand diameter was used for k_s at the bottom of the main channel, but it did not include the resistance due to sand wave.

Table 4. Conditions for analysis

Case	Discharge (l/s)	Main Channel depth (cm)	Flood Channel depth (cm)	Relative Depth Dr
4	35.9	8.0	2.5	0.31
5	63.7	10.6	5.3	0.49

Table 4 gives the conditions for the numerical analysis. The conditions were decided to produce a depth (i.e., relative depth) equivalent to that used in the experiment, and the resistance coefficient was fixed so that the calculated discharge would match the experimental discharge.

(2) Bed deformation

Figs.20 and 21 show the observed and calculated bed shapes by contour lines for Case 4, respectively. Figs. 22 and 23 show similar results for Case 5. In both the cases the flow proceeds from the left to the right. The observed results show the bed shape of one wave-length in the central part of channel.

Comparing Fig. 22 with Fig. 23, the calculated scouring occurs continuously from the inner bank to the next inner bank at the maximum curvature and the calculated result is similar to the observed one. On the other hand, the bed shape in Figs. 21 does not agree well with one in Fig. 20. In the observed results, bed scouring occurs at the maximum curvature. In the calculated results, a scouring region spreads out from the outer bank to the inner bank and the maximum scouring occurs near the bank at the maximum curvature. This means that the observed bed shape in Dr=0.49 has the characteristics of a compound meandering flow but the calculated bed shape in Dr=0.31 displays one of a single-section meandering flow.

Generally, the bed shape changes from one in a single section meandering channel to one in a compound meandering channel around where the relative depth becomes 0.3 (Fukuoka, et al., 1997c). However, this transition of bed shape is sensitive to the roughness of bed and so on. The river bed can take both shapes to this relative depth. When the effects of the secondary flow mentioned in the

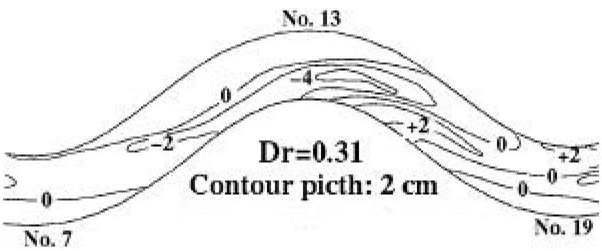

Fig. 20. Bed variation contour in Case 4.
(Observed results)

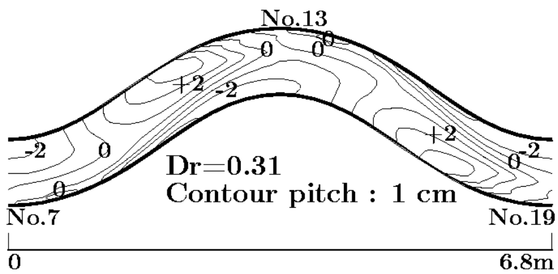

Fig. 21. Bed variation contour in Case 4.
(Calculated results)

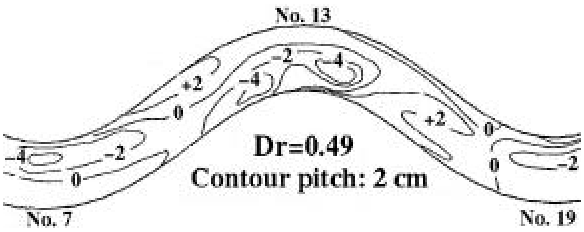

Fig. 22. Bed variation contour in Case 5.
(Observed results)

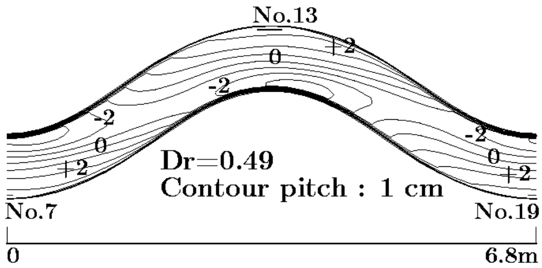

Fig. 23. Bed variation contour in Case 5.
(Calculated results)

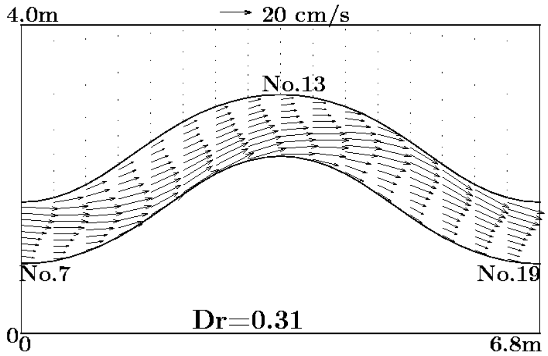

Fig. 24. Calculated vector of depth-averaged velocity below flood channel height in Case 4.

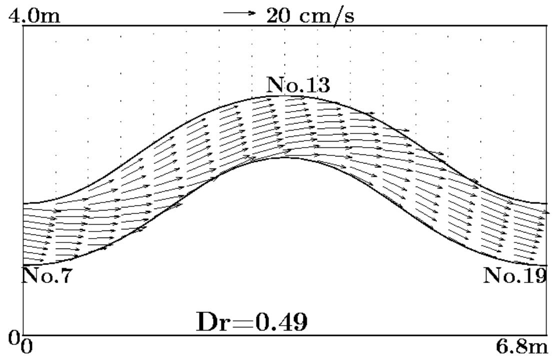

Fig. 26. Calculated vector of depth-averaged velocity below flood channel height in Case 5.

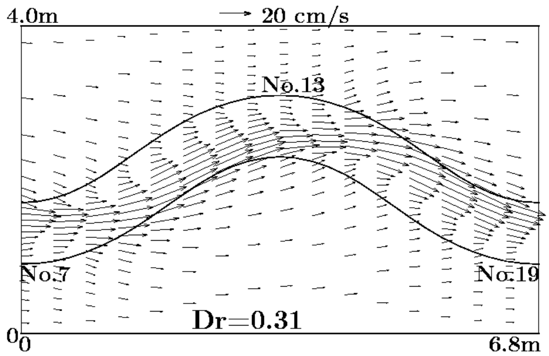

Fig. 25. Calculated vector of depth-averaged velocity above flood channel height in Case 4.

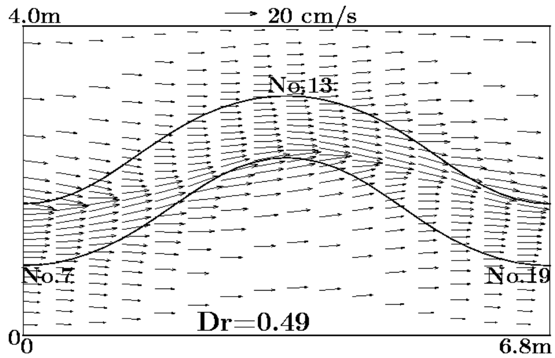

Fig. 27. Calculated vector of depth-averaged velocity above flood channel height in Case 5.

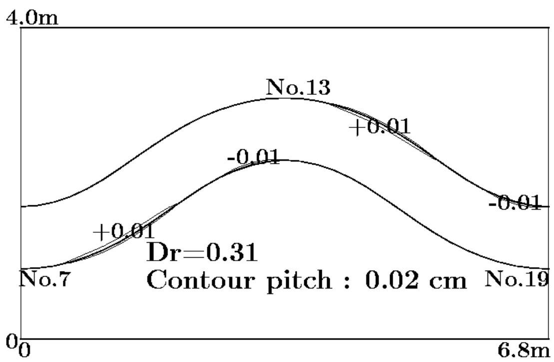

Fig. 28. Calculated depth-averaged pressure deviation below flood channel height in Case 4.

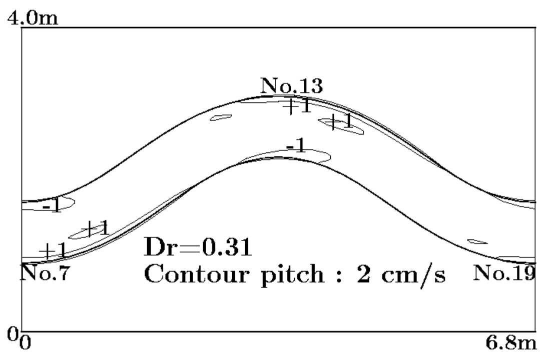

Fig. 30. Calculated vertical velocity at the height of flood channel in case 4.

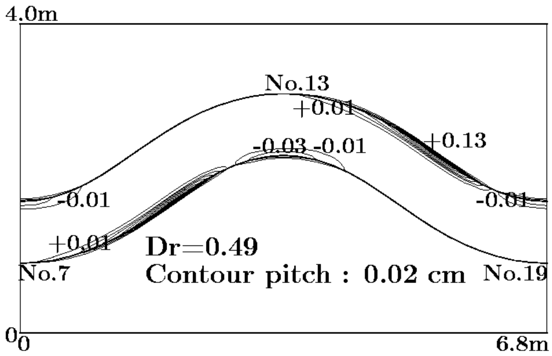

Fig. 29. Calculated depth-averaged pressure deviation below flood channel height in Case 5.

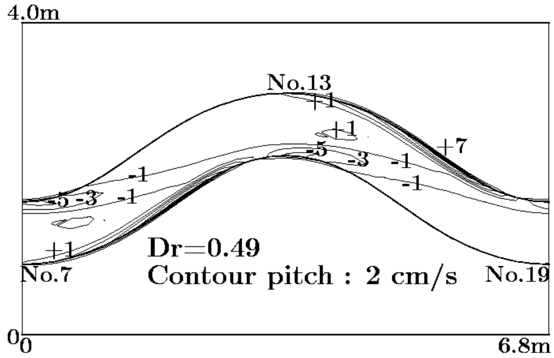

Fig. 31. Calculated vertical velocity at the height of flood channel in Case 5.

following section surpass the effects of the longitudinal change in the tractive force for the bed deformation, the bed shape becomes one in a compound meandering channel. The slight difference between observed and calculated results for the scouring position is due to the difference of bed roughness and the use of periodic boundary conditions for the experimental results which were not actually periodic.

(3) Characteristics of flow field

Figs. 24 and 25 show the calculated velocity vectors at below and above flood channel height respectively for Case 4. Figs. 26 and 27 show similar results for Case 5. As shown in Fig. 24, flow below flood channel height concentrates near the inflection point of outer bank and scouring occurs there. On the contrary in Fig. 26, flow dose not so concentrate and the change in velocity is small. But, the flow over bed goes towards the outer bank and bed materials move to the bank by this secondary flow. As shown in Fig. 25 (Dr=0.31), the main flow above the height of flood channel proceeds along the main channel. The velocity over the flood channel is small and the velocity changes considerably in the transverse direction. But, the momentum exchange between flow in main channel and above flood channel is small, as the exchange in rate of flow is small in small relative depth. On the contrary in Fig. 27, flow goes along the levee of flood channel and the velocity above flood channels is large. Comparing Figs. 26 and 27, the direction of the secondary flows is reversed from one observed in a single section meandering flow.

Figs. 28 and 29 show the distribution of calculated pressure deviation for case 4 and 5 respectively. When the relative depth is small, the pressure deviation in a main channel below the height of flood channel is small and pressure is almost hydrostatic condition. When the relative depth is large, however, the pressure deviation is large near the bank around the inflection point and the apex of meandering.

Figs. 30 and 31 show the distribution of calculated vertical velocity at the height of flood channel for case 4 and 5 respectively. As shown in Fig. 31, flow rise up near the bank around the inflection point from lower channel and goes down to lower channel around apex. These places exist where the change in the pressure intensity is large. In Fig. 30, the large vertical velocity is not seen. Comparing Figs. 26 and 31, we can find that the faster flow goes down into lower channel and is diverging over the bed. At the same time Fig. 23 indicates that the bed scouring occurs continuously over the area where the faster flow goes down. The tractive force is larger over the area where the fast flow goes down and flow goes out of this area with bed materials. Therefore, in this area the bed scoring occurs.

4 Concluding Remarks

Rivers generally possess irregular plan and cross-sectional forms. It has been known that the flood flow is stored in the river courses due to the effects of unsteadiness and channel resistance of the flood flow as it proceeds downstream. It is, however, hard to measure and assess a storage volume by means of the present technique for flood discharge measurement. For this reason, we cannot consider properly its storage capacity for flood control plan of a river.

In this paper together with the other paper (Fukuoka, et al., 2000), an assessment of a storage volume and peak discharge attenuation of the flood flow is attempted mainly by the laboratory experiment.

Technical knowledge found in this investigation seems to be useful for flood control and river environment in relation to river course design and river's vegetation management.

The present river planning should be re-examined from the standpoint of the storage volume and peak discharge attenuation, which is an essential function of natural rivers. To perform this plan steadily, we have to begin with the proper observation of temporal longitudinal water surface profiles and discharge in a representative reach during floods.

Main conclusions in the paper are summarized as:

(1) In an unsteady compound meandering flow, surface slope changes greatly during flooding because of the resistance characteristics associated with the flood flow's unsteadiness and the channel's plan and cross-sectional forms, thereby resulting in channel storage and an accompanying attenuation of peak discharge.

(2) The increase in flow resistance caused by riparian vegetation greatly changes surface slope during flooding, slowing propagation of the flood waves. The result is increased channel storage and attenuation of the peak discharge.

(3) When the relative depth of compound meandering channels is low, the characteristics of the flow resemble those of a single-section meandering channel. For this case, the deviation of pressure intensity from the hydrostatic pressure distribution is relatively small, therefore the hydrostatic pressure approximation is at some degree reasonable. When the relative depth is high, the deviation of pressure intensity from hydrostatic pressure distribution is large and the results with the hydrostatic pressure approximation can not represent the observed flow and bed topography in laboratory experiments.

(4) The numerical analysis has shown the importance of secondary flow structures in the formation of the bed features. When the relative depth is high, the flow from the flood channel enters the main channel producing the secondary flow with an inverse rotation to the one observed in curved channels

with single cross sections. This secondary flow goes toward the bed at the inner bank. As results, scouring occurs at the inner bank. On the contrary, deposition occurs at the outer bank.

References

1) Ashida, K., S. Egashira, B. Liu and M. Takiguchi, "Flow characteristics and bed variations in a meandering channel with flood-plains", Annuals Disaster Prevention Research Institute, Kyoto University, No.32B-2, pp. 527-551, 1989.

2) Ashida, K., S. Egashira, and B. Liu, "A study of the hydraulics of meandering compound channel flows", Proceedings of the Hydraulic Engineering, JSCE, Vol. 34, pp. 397-402, 1990.

3) Ven Te Chow V.T.: "Open Channel Hydraulics", McGraw-Hills, Chapter 20, pp.586-609, 1956.

4) Flood Control Division, Ministry of Construction, and Public Works Research Institute, Ministry of Construction, "Study on river characteristics", Annual Meeting of Construction Technology, Vol.40, pp.1-3, 1986.

5) Fukuoka, S. and M. Yamasaka, "Alternating bars in a straight channel", Proc. of the 27th Japanese Conference on Hydraulics, pp. 703-708, 1983.

6) Fukuoka, S., A. Watanabe, Y. Kayaba and H. Soda, "Flow and bed profiles in curved channels with discontinuously installed vanes", Journal of Hydraulic, Coastal and Environmental Engineering, JSCE, No. 479/II-25, pp.61-70, 1993.

7) Fukuoka, S., H. Miyazaki, H. Ohgushi, and D. Kamura, "Flow and bed topography in a meandering compound channel with phase difference between the alignment of the main channel and levee", Annual Journal of Hydraulic Engineering, JSCE, Vol. 40, pp. 941-946, 1996.

8) Fukuoka, S., H. Ogushi, D. Kamura, and S. Hirao, "Hydraulic characteristics of the flood flow in a compound meandering channel ", Journal of Hydraulic, Coastal and Environmental Engineering, JSCE, No. 579/II-41, pp. 83-92, 1997a.

9) Fukuoka, S., A. Watanabe, D. Kamura, and S. Okada, "Study of rate of bed load and bed topography in a meandering compound channel", Annual Journal of Hydraulic Engineering, JSCE, Vol. 41, pp. 883-888, 1997b.

10) Fukuoka, S., H. Takahashi and D. Kamura, "Compound meandering flow and simple meandering flow in compound meandering rivers－analysis by the use of aerophotograph flood flow velocity vector", Annual Journal of Hydraulic Engineering, JSCE, Vol. 41, pp. 971-976, 1997c.

11) Fukuoka, S. and A. Watanabe, "Three dimensional analysis on flows in meandering compound channels", Journal of Hydraulic, Coastal and Environmental Engineering, No.586/II-42, pp.39-50, 1998.

12) Fukuoka, S., "New horizons of flood flow hydraulics and fluvial hydraulics", Lecture notes of the 35th Summer Seminar on Hydraulic Engineering, 1999,Course A, pp. A-2-1 ~ A-2-25, 1999.

13) Fukuoka, S., A.Watanabe, H.Okabe and K.Seki; "Effects of unsteadiness, planform and cross-sectional form of channels on hydraulic characteristics of flood flows", Annual Journal of

Hydraulic Engineering, JSCE, Vol.44, pp.867-872, 2000.

14) Kinoshita, R., "Experimental study concerning field work of alluvial phenomena at flooding and best possible river course example", Control of Flood Flows in Fluvial Rivers and Improvement of Safety of River Channel during Flood, Report of Scientific Research Fund, No. A-62-1, pp. 63-168, 1988.

15) Mori, A. and T. Kishi, "The characteristics of river bed topography of Ishikari-river observed on the Flood in 1981", Proc. of the 30th Japanese Conference on Hydraulics, pp.493-498, 1986.

16) Muto, Y., K. Shiono, H. Imamoto, and T. Ishigaki, "3-dimensional structure for overbank flow in meandering channel", Annual Journal of Hydraulic Engineering, JSCE, Vol. 40, pp. 711-716, 1996.

17) Sellin, R.H.I., Ervine, D.A.and Willets, B.B.,"Behaviour of meandering two-stage channels, Proc.Instn Civ.Engrs. Wat, Marit. and Energy, 101,pp.99-101, 1993.

18) Watanabe, A. and S. Fukuoka, "Three dimensional analysis on flows and bed topography in a meandering compound channel", Annual Journal of Hydraulic Engineering, JSCE, Vol. 43, pp. 665-670, 1999.

19) Willets, B. B. and R. I. Hardwick, "Stage dependency for overbank flow in meandering channels", Proc. Instn Civ.Engrs Wat, Marit. and Energy, 101, pp.45-54, 1993.